Theoretical studies of the HO+O⇔HO 2 ⇔ H+O 2 reaction. II. Classical trajectory calculations on an ab initio potential for temperatures between 300 and 5000 K

J. Troe and V. G. Ushakov

Citation: The Journal of Chemical Physics **115**, 3621 (2001); doi: 10.1063/1.1388201
View online: http://dx.doi.org/10.1063/1.1388201
View Table of Contents: http://scitation.aip.org/content/aip/journal/jcp/115/8?ver=pdfcov
Published by the AIP Publishing

Theoretical studies of the HO+O⇔HO_2⇔H+O_2 reaction. II. Classical trajectory calculations on an *ab initio* potential for temperatures between 300 and 5000 K

J. Troe[a] and V. G. Ushakov[b]
Institut für Physikalische Chemie, Universität Göttingen, Tammannstrasse 6, D-37077 Göttingen, Germany

(Received 10 April 2001; accepted 6 June 2001)

A comparably simple new analytical expression of the potential energy surface for the HO+O⇔HO_2⇔H+O_2 reaction system is designed on the basis of previous high precision *ab initio* calculations along the minimum energy path of the HO_2→H+O_2 and HO_2→HO+O dissociations. Thermal rate constants for the reaction HO+O→H+O_2 are determined by extensive classical trajectory calculations. The results depend on the policy to solve the zeropoint energy problem. We show that, with the chosen policy, there are nearly equal amounts of statistical and nonstatistical backdissociations HO+O←HO_2 following HO+O→HO_2; however, backdissociations become important only at temperatures above about 500 K. Below 500 K, the reaction is completely capture-controlled. Below 300 K, classical trajectory treatments become inadequate, because quantum effects then are so important that only the quantum statistical adiabatic channel model gives reliable results. For the reaction HO+O→H+O_2 and the range 300–5000 K, a rate constant of $k/10^{-11}\,\mathrm{cm^3\,molecule^{-1}\,s^{-1}} = 0.026(T/1000\,\mathrm{K})^{1.47} + 1.92(1000\,\mathrm{K}/T)^{0.46}$ is obtained from the trajectory calculations. Converting experimental results for the reaction H+O_2→HO+O to the reverse reaction on the basis of the revised enthalpy of formation of OH, agreement between experiment and theory within better than 20% is obtained between 300 and 5000 K. © *2001 American Institute of Physics.* [DOI: 10.1063/1.1388201]

I. INTRODUCTION

Because of its central importance in combustion chemistry (see, e.g., Ref. 1), the rate of the reaction

$$(k_1)\quad \mathrm{H+O_2 \rightarrow HO+O} \tag{1.1}$$

needs to be known with the largest possible accuracy under combustion conditions. Likewise, the rate of the reverse reaction

$$(k_2)\quad \mathrm{HO+O \rightarrow H+O_2}, \tag{1.2}$$

because of its importance in atmospheric and interstellar chemistry (see, e.g., Ref. 2), should be known down to very low temperatures. An internally consistent picture requires the understanding of both k_1 and k_2 which are linked by the equilibrium constant,

$$K_{\mathrm{eq}} = k_1/k_2. \tag{1.3}$$

In addition, a series of other quantities such as the high pressure recombination rate constant of the reaction,

$$(k_4)\quad \mathrm{H+O_2(+M) \rightarrow HO_2+(M)}, \tag{1.4}$$

and detailed scattering cross sections for process (1.1) are related and should be analyzed together with k_1 and k_2.

Extensive experimental and theoretical studies over the last decades have led to converging results, the agreement generally being of the order of about a factor of 2, even when very crude theoretical models were applied. This accuracy has been achieved with a variety of methods, for summaries of experimental work see, e.g., Refs. 3–6, for theoretical work see Refs. 1, 7, 8. Going beyond the factor of 2 accuracy, such as this is urgently required for combustion applications, is a more demanding task. At first, the thermodynamic data of the species involved should be well established. The enthalpy of formation of OH, e.g., recently has been questioned again and revised down by about 2 $\mathrm{kJ\,mol^{-1}}$ to a value of $\Delta H^0_{f,0} = 36.94(\pm 0.38)\,\mathrm{kJ\,mol^{-1}}$;[9] relating k_1 and k_2 through Eq. (1.3) certainly requires reliable thermodynamic data. An expression of

$$K_{\mathrm{eq}} = 17.0 \times (T/1000\ \mathrm{K})^{-0.213} \exp(-8144\ \mathrm{K}/T) \tag{1.5}$$

over the range 1000–5000 K seems to be the presently best choice.[10] Improving measurements of k_1 over the temperature range 1000–5000 K and reconciling data from different laboratories has led to a recommendation[11] of

$$k_1 = 1.62(\pm 0.12) \times 10^{-10} \exp[-(7474 \pm 122)\mathrm{K}/T]\ \mathrm{cm^3\,molecule^{-1}\,s^{-1}} \tag{1.6}$$

for the measurements from Refs. 11–14. The latest measurements of k_2,[15,16] now cover the temperature range 160–500 K. Recent cross-section measurements for reaction (1.1) from Ref. 17 have corrected down earlier higher values in an intermediate range of translational energies and now cover energies between 1 and 2.5 eV.

On the theoretical side, higher precision requires better potential energy surfaces, with optimum accuracy in all ki-

[a]Author to whom correspondence should be addressed.
[b]Present address: Institute of Problems of Chemical Physics, Russian Academy of Sciences, 142432 Chernogolovka, Russia.

netically relevant places. The DMBE IV surface by Varandas and co-workers[18] and the DIM surface by Kendrick and Pack[19] provided progress over the very early Melius and Blint potential.[20] The DMBE IV surface has been used over many years now for a series of dynamical studies. *Ab initio* calculations from medium to higher[8,21–23] precision, however, revealed (see Ref. 24, and this work) some inaccuracies of the DMBE IV potential, which at first sight appear minor, but which become unacceptable when one is heading for the 10% accuracy of kinetic data.

The dynamics of reactions (1.1), (1.2), and (1.4) has been analyzed by a variety of methods such as classical trajectories (CT), the statistical adiabatic channel model (SACM), partly in combination with CT treatments of the capture parts of reactions (1.1) and (1.2), and time-dependent wave packet calculations. We do not intend to review the merits of the various approaches at this place, reference to earlier work being made in the cited articles. Instead we try to provide an improved CT treatment on an *ab initio* surface which avoids some of the problems of earlier work. With this approach we find agreement with measurements of k_1 and k_2 between 300 and 5000 K on a 10%–20% precision level.

Essential aspects of our approach are the following:

(i) Reaction (1.2) cannot be described by CT calculations at temperatures below 300 K, because the large rotational constant of OH and the open electronic shell character of OH and O requires a quantum treatment.[25] Since reaction (1.2) at $T \leqslant 300\,\mathrm{K}$ apparently is completely capture-controlled (i.e., no back-dissociation of the intermediate HO_2, see below), rigorous SACM probably provides an adequate description, see part I of this series.[8] We further elaborate this quantum range in part III of this series.[26]

(ii) Our SACM/CT treatment in Ref. 8 showed that **statistical** backdissociation of HO_2 to HO+O in reaction (1.2) only sets in at $T \geqslant 500\,\mathrm{K}$. Since we found agreement between our SACM/CT results and experimental determinations of k_2 up to 500 K, we concluded that there is no evidence for **nonstatistical** backdissociation. However, on the basis of CT calculations on the DMBE IV potential, about 50% backdissociation in Ref. 27 was postulated to be present between 200 and 5000 K. We, therefore, had to come back to the question of nonstatistical backdissociations. Doing complete CT calculations on our new *ab initio* surface, we come to the conclusion that our earlier assumption may have been premature. While in contrast to Ref. 27 we conclude that there is only little statistical and nonstatistical backdissociation at $T \leqslant 500\,\mathrm{K}$, we find that substantial amounts of nonstatistical backdissociation in addition to statistical backdissociation appear at $T \geqslant 500\,\mathrm{K}$. We investigate the reasons for the differences in the conclusions about backdissociation between this work and Ref. 27. We find that different policies to solve the zero point energy (ZPE) problem in CT calculations are responsible for different conclusions about the extent of backdissociations; differences of the potentials are shown to be only of minor importance in this respect.

(iii) We demonstrate that differences between the present *ab initio* and the DMBE IV potential at some temperatures can lead to substantially different capture rate constants $k_{2,\infty}$ of reaction (1.2) and $k_{4,\infty}$ of reaction (1.4), at other temperatures cancelling compensations can lead to similar results. In particular, we identify different minimum energy path (MEP) potentials and different anisotropies of the two potential models. We also demonstrate that two-dimensional rigid rotor and three-dimensional nonrigid rotor CT calculations lead to identical capture rates.

(iv) The zero point energy problem of the CT calculations can confidently be overcome only by comparison with full time-dependent wave packet calculations. Such calculations slowly are approaching a quantitative level.[28–30] However, even the latest of these calculations are still incomplete; in addition, so far they have only been done on potentials of the DMBE IV quality.[30] New, more extended, quantum scattering calculations, therefore, should be done with the more accurate potentials.

In the following we first provide an analytical representation of a complete potential which is based on the *ab initio* calculations from Refs. 8 and 31; this new potential is then compared with the DMBE IV potential from Ref. 18. We next present full CT calculations in comparison to our earlier statistical SACM/CT treatment from Ref. 8. We analyze the consequences of different policies to handle the zero point energy problem. We finally compare our theoretical results with experiments for $T \geqslant 300\,\mathrm{K}$, leaving the quantum range $T \leqslant 300\,\mathrm{K}$ to part III.[26]

II. ANALYTICAL REPRESENTATION OF AN *AB INITIO* POTENTIAL

The statistical SACM/CT calculations for reactions (1.2) and (1.4) from Refs. 8 and 31 did not require analytical representations of a global potential but only involved the MEP potentials and the anisotropies in the vicinity of the MEPs of the HO+O and $H+O_2$ approaches. In the present fully dynamical CT treatment of reaction (1.2) the situation changes and a global potential is required. We construct this on the basis of the *ab initio* results described in Ref. 31 for the $H+O_2$ side and in Ref. 8 for the HO+O side. We use the previously derived representations for the $H+O_2$- and HO+O-sides and combine them by a switching technique. The result is of comparably simple form, being less complicated than the DMBE IV expression. The given analytical potential certainly does not represent all ranges of the potential equally well but, by focussing on the MEP potential and the anisotropies in the vicinity of the MEPs, it is probably most suited for the reactions considered here.

A. Representation of the H–OO potential

We use center-of-mass (c.o.m.)-coordinates, r denoting the distance between H and the c.o.m. of O_2, γ being the angle between the line connecting the c.o.m.s and the axis of O_2. The potential $V_{\mathrm{H-OO}}(r,\gamma)$ is approximated in the form,[31]

$$V_{\mathrm{H-OO}}(r,\gamma) = V(r) + C(r)[\cos^2\gamma - \cos^2\gamma_0(r)]^2 \quad (2.1)$$

with

$$V(r) = -d_0\left(\sum_{i=0}^{6} c_i x^i\right)\exp(-c_1 x) + A/y^2 - 2A/y, \quad (2.2)$$

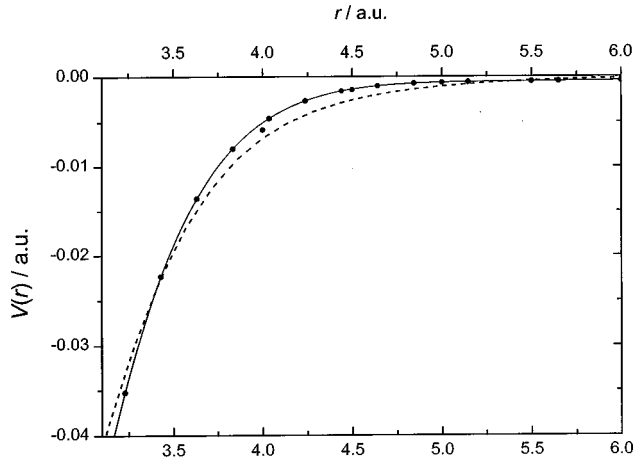

FIG. 1. MEP potential $V(r)$ of the H–OO interaction [r=H–OO c.o.m. distance, r and V in atomic units $a_0=0.529$ Å and $E_h=2625.5$ kJ/mol; ●=*ab initio* points from Ref. 31, full line=analytical representation of *ab initio* points by Eq. (2.2), dashed line=DMBE IV potential from Ref. 18].

where $x=r-r_e$, $y=(r/r_e)^6$, $c_0=1$, $c_1=3.944\,54$, $c_2=12.477\,92$, $c_3=18.929\,74$, $c_4=-44.611\,70$, $c_5=26.808\,32$, $c_6=-9.688\,18$, $A=0.065\,660$, $d_0=0.022\,756$, and $r_e=2.477\,8$ (all quantities in atomic units $a_0=0.529$ Å and $E_h=2625.50$ kJ/mol). In addition, we have

$$\cos\gamma_0(r)=0.63+0.37\{1+\exp[-2.25(r-8.3)]\}^{-1}+0.37\exp(-0.75r) \tag{2.3}$$

and

$$C(r)=0.13129r^{1.5}\exp(-0.35r)/[1+(0.2688r)^9]. \tag{2.4}$$

MEP potential, geometry, and anisotropy are represented graphically in Figs. 2–4 of Ref. 31, demonstrating the excellent agreement between analytical representation and *ab initio* points. In Figs. 1 and 2 we reproduce the comparison of the MEP potentials from Ref. 31 and the present work, and the DMBE IV potential such as given in Ref. 24. The differences in the attractions at various distances in part have compensating effects on the capture rate constants $k_{4,\infty}$;[32] however, at lower temperatures ($T\leqslant 300$ K), the different long-range behavior leads to markedly different low temperature values of $k_{4,\infty}$. This applies to a temperature range where quantum effects, such as treated by SACM, are not yet relevant in reaction (1.4).

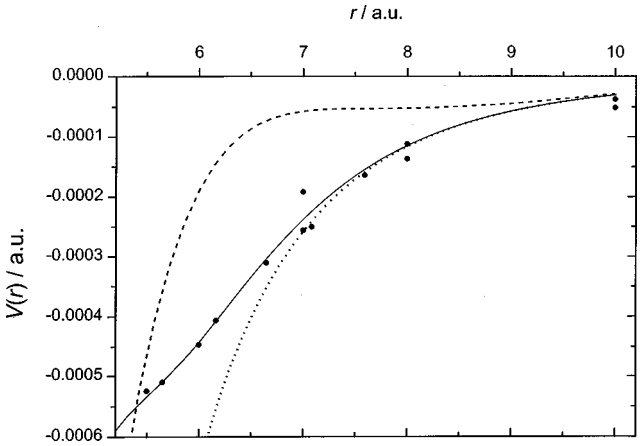

FIG. 2. As Fig. 1, at larger values of r. In addition the dotted line shows the asymptotic potential $V(r)=-30.4$ a.u. $(r/\text{a.u.})^{-6}$.

B. Representation of the HO–O potential

Now denoting by r the c.o.m.-distance between HO and O, and by γ the angle between the line connecting the c.o.m.s and the axis of HO, the potential $V_{\text{HO–O}}(r,\gamma)$ is represented by[8]

$$V_{\text{HO–O}}(r,\gamma)=V(r)+d_2(r)x^2+a(r)x^3+b(r)x^4 \tag{2.5}$$

with

$$x=\cos\gamma-\cos\gamma_0(r) \tag{2.6}$$

and

$$\cos\gamma_0(r)=0.122\,72-1.881\,02r\exp(-0.9677r). \tag{2.7}$$

In addition, we have (again in atomic units),

$$V(r)=-d_0\left[\sum_{i=0}^{5}c_i(r-r_e)^i\right]\exp[-c_1(r-r_e)] \tag{2.8}$$

with $c_0=1$, $c_1=2.648\,13$, $c_2=1.615\,899$, $c_3=0.078\,282\,5$, $c_4=-0.667\,750\,5$, $c_5=0.330\,579$, $d_0=0.108\,77$, and $r_e=2.568$,

$$d_2(r)=0.199\,37\exp[-4.2047(r/5)^{3.1}]; \tag{2.9}$$

$$a(r),b(r)=\left[\sum_{i=1}^{6}\delta_i(x-x_0)^i\right]\exp[-\beta(x-x_0)]\times\{1+\exp[-1.75\beta(x-x_0)]\}^{-1}, \tag{2.10}$$

with $x=\ln(r)$ and with $\delta_1=-0.081\,35$, $\delta_2=-0.792\,22$, $\delta_3=3.046\,73$, $\delta_4=-26.671\,24$, $\delta_5=48.215\,06$, $\delta_6=-37.838$, $\beta=10.581\,59$, and $x_0=1.657\,67$ for the function $a(r)$, and with $\delta_1=-0.000\,79$, $\delta_2=1.037\,28$, $\delta_3=-7.214\,75$, $\delta_4=40.580\,28$, $\delta_5=-69.242\,1$, $\delta_6=50.166\,06$, $\beta=10.904\,77$, and $x_0=1.655\,97$ for the function $b(r)$, respectively. One should note that Eqs. (2.5)–(2.10) only apply to the lowest $^2A''$ electronic state of HO_2 (for the higher $^2A'$ state, see Ref. 8). A comparison between *ab initio* points and the analytical representation is given in Ref. 8; equipotential lines from our analytical representation and the DMBE IV potentials, such as given in Figs. 4 and 5 of Ref. 8, show a quite similar general shape. The differences are again in the finer details. Figures 3 and 4 show the MEP potentials from the present and the DMBE IV potential. Again the differences of the MEP potentials have partly compensating effects for the capture rate constants of reaction (1.2) which we denote by $k_{2,\infty}$. In this case, however, in contrast to reaction (1.4) characterized by the potential from Eqs. (2.1)–(2.4), less pronounced anisotropies of the DMBE IV potential lead to higher capture rate constants than in the present work, such as shown below.

C. Switching potential near H–O–O

In the following, we combine the potentials from Secs. II A and II B to a global potential surface. We denote the two OH diatomics in HOO by A and B, with O–H distances "a"

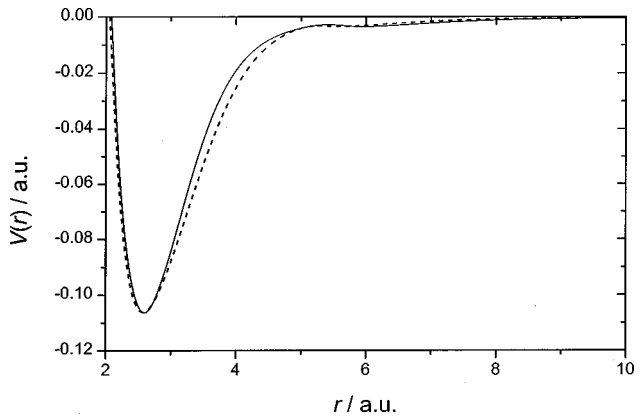

FIG. 3. MEP potential $V(r)$ of the HO–O interaction [r=HO–O c.o.m. distance, full line=analytical representation of *ab initio* points from Ref. 8 by Eq. (2.8), dashed line=DMBE IV potential from Ref. 18].

and "*b*," respectively, and the OO diatomic by C with an O–O distance "*c*." We then define three-dimensional (3D) potentials by

$$f_A(a,b,c)=V_{\mathrm{HO-O}}(r_A,\gamma_A)+M_{\mathrm{OH}}(a),$$
$$f_B(a,b,c)=V_{\mathrm{HO-O}}(r_B,\gamma_B)+M_{\mathrm{OH}}(b), \qquad (2.11)$$
$$f_C(a,b,c)=V_{\mathrm{H-OO}}(r_C,\gamma_C)+M_{\mathrm{OO}}(c),$$

where r and γ as before correspond to the c.o.m. distances and angles of the respective diatom–atom combinations. The quantities M are Morse potentials,

$$M=D\{\exp[-2\beta(r-r_e)]-2\exp[-\beta(r-r_e)]\}, \qquad (2.12)$$

with $\{D,\beta,r_e\}=\{0.191\,570,\ 1.409\,7,\ 2.54\}$ for O_2 and $\{0.169\,872,\ 1.224\,1,\ 1.85\}$ for HO, respectively (all in atomic units as before). With these data and a small change of the parameter d_0 in Eq. (2.8) from 0.108 77 to 0.110 114, the same energy and geometry at the equilibrium configuration of HO_2 were achieved for all three potentials of Eq. (2.11).

The global 3D-potential $V_{\mathrm{HOO}}(a,b,c)$ then is composed by the potentials of Eq. (2.11) with weight functions in the following form:

$$V_{\mathrm{HOO}}(a,b,c)=(w_Af_A+w_Bf_B+w_Cf_C)/(w_A+w_B+w_C), \qquad (2.13)$$

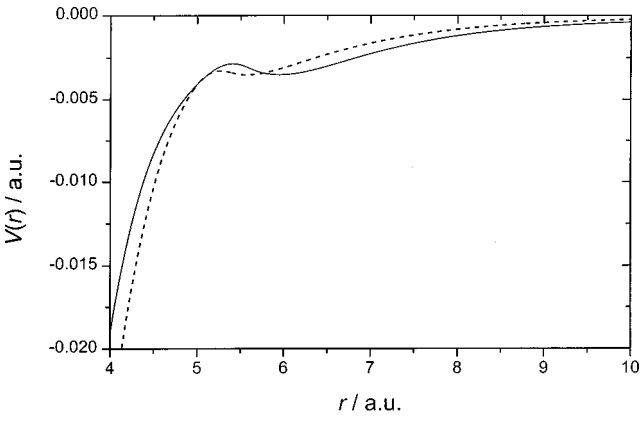

FIG. 4. As Fig. 3, enlarged.

where

$$w_A=\exp[-75(a-1.85)^2/bc],$$
$$w_B=\exp[-75(b-1.85)^2/ac], \qquad (2.14)$$
$$w_C=\exp[-130(c-2.54)^2/ab].$$

The 3D-potential $V_{\mathrm{HOO}}(a,b,c)$ has accurate MEP properties along the H–OO and HO–O paths and nearly reproduces the correct energy and geometry of the equilibrium configuration of HO_2. The parameters 75 and 130 in Eq. (2.14) were obtained by comparison with the DMBE IV potential in the vicinity of the HO_2 equilibrium configuration. In some of our calculations we improved the quality of the potential near to the HO_2 equilibrium configuration by replacing r_e, in the function M from Eq. (2.12) for O_2, by putting

$$r_e=2.2828+0.5164/\{1+\exp[0.8(r_c-2.4778)]\}. \qquad (2.15)$$

The parameter 75 in Eq. (2.14) then was also changed into 60. Making β in Eq. (2.12) an r-dependent function could further improve $V_{\mathrm{HOO}},(a,b,c)$ near to the equilibrium configuration of HO_2. However, we found no significant effect of these improvements on our CT calculations.

III. CLASSICAL TRAJECTORY CALCULATION

Details of our CT calculational method have been described before[8,31,33] such that only few details will be specifically mentioned in the following. We always followed a sufficiently large number of trajectories such that statistical scatter became negligible, i.e., being in the 2% range. In the present case, about 10^4 trajectories were followed for each point at a given temperature.

A. 3D versus 2D capture calculations

Our previous SACM/CT calculations of capture rates have been made treating O_2 in reaction (1.4), and HO in reaction (1.2), as rigid rotors, with atom–atom distances kept at their equilibrium distances in the vibrational ground state. We argued that the problem of zero point energy (ZPE) and quantization of the vibrations for capture processes in this way could be circumvented. In a recent communication commenting on our work on reaction (1.4),[32] this policy was questioned with the argument that "2D-trajectories" would sample a smaller part of the global potential than "3D-trajectories" employing nonrigid rotors. Using the present global potential we have tested 2D versus 3D-CT capture calculations, at first for reaction (1.4) $H+O_2\rightarrow HO_2$ and then for the capture part of reaction (1.2) $HO+O\rightarrow HO_2$. In no case we found differing results. We demonstrate this in Fig. 5 for $HO+O\rightarrow HO_2$, where the geometrically complicated MEP with a double minimum potential should provide a particularly sensitive test. The agreement between 2D and 3D results at $T\geqslant 300$ K is perfect, confirming that the capture dynamics is indeed governed by the MEP potential and the anisotropy in the vicinity of the MEP. The dashed lines are from our previous SACM/CT study (part I, Ref. 8), the upper corresponding to capture ($k_{2,\infty}$), the lower corresponding to the complete reaction (1.2) (k_2). The latter curve is included for comparison, demonstrating the amount of statistical backdissociation to be discussed below. We have tested some

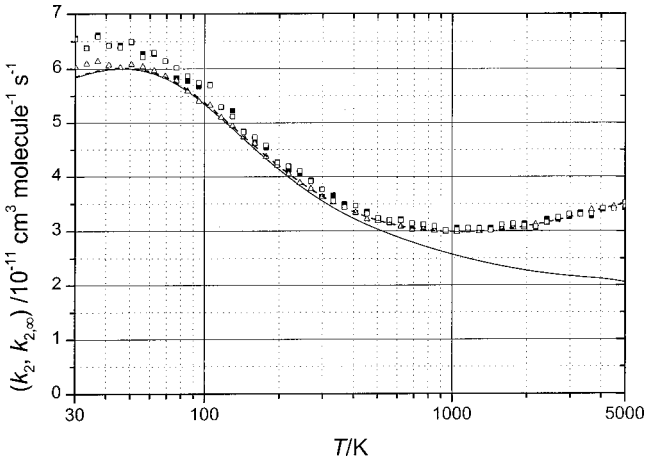

FIG. 5. CT calculations of the rate constants for capture ($k_{2,\infty}$) and for full reaction (k_2) of reaction (1.2). (Dashed line=$k_{2,\infty}$ from 2D calculations of Ref. 8, full line=k_2 from statistical 2D calculation of Ref. 8, ■=3D calculation of $k_{2,\infty}$ from this work with vibrationless OH, □=3D calculation of $k_{2,\infty}$ from this work with thermally vibrating OH, Δ=2D calculation of $k_{2,\infty}$ with potential from this work.)

alternative policies about how to handle the HO rotor which led to slightly differing results at $T \leqslant 300$ K. In the nonrigid rotor calculations we either put no vibrational energy or thermal classical vibrational energy into the HO oscillator. Within the calculational scatter of 2% this had no effect. The 3D calculations at the lowest temperatures led to slightly higher results than the 2D calculations because the effective rotational constant of HO from the global potential was slightly different from the literature values such as used in the 2D SACM/CT treatment. We also tested two versions of the latter with different summations over numbers of open channels which led to very minor differences at $T \leqslant 50$ K, where major quantum corrections have to be made anyway, see parts I and III. In conclusion, 2D and 3D calculations lead to identical capture rates.

B. Nonstatistical versus statistical backdissociation

Figure 5 includes the statistical SACM/CT calculations for k_2 from the combined 2D calculations of H+O$_2$ and HO+O capture rate constants described in part I.[8] This statistical treatment is only mildly influenced by the ZPE problem of the CT calculations. In the following, we describe fully nonstatistical classical trajectory calculations of k_2 on the present global potential energy surface. In doing this, like in all previous CT calculations, unavoidly we encounter the ZPE dilemma.

In order to cope with the ZPE problem we adopted the following strategy. At first, we started CTs from the HO+O-side with an initial vibrational energy of HO equal to the ZPE. Part of the CTs led to long-lived HO$_2$ complexes dissociating either to H+O$_2$ or to HO+O. Another part of the CTs led to short HO$_2$ encounters with substantial backdissociation to HO+O. Figures 6 and 7 illustrate the two different types of HO+O encounters. In both cases, part of the HO emerging from the encounter contained less than the ZPE. It appears plausible to reject these forbidden CTs and only to retain those CTs which lead to HO with vibrational excitation larger than the ZPE. Below we compare the fractions of allowed backdissociations from the nonstatistical full CT and the statistical SACM/CT treatment. Before doing this, we mention the second possibility to exclude forbidden trajectories: We started CTs from the HO+O-side without any vibrational excitation of HO. In this case, backdissociation can only lead to vibrational excitation of HO. The two alternatives lead to very similar results such as illustrated in Fig. 8. For this figure, we have calculated the allowed total fraction of encounters which lead to back-dissociation and subtracted the statistical fraction such as calculated in part I. The figure thus shows the allowed nonstatistical fraction of encounters leading to backdissociation. Neglecting the ZPE problem, one would have a nonstatistical fraction which from values near 0.33 at 30 K increases to values near 0.45 at 3000 K. Excluding the forbidden trajectories, or starting only from vibrational energies of HO equal to zero, there is no backdissociation below 100 K, about 8% at 300 K, 15% at 500 K, and about 40% at 3000 K.

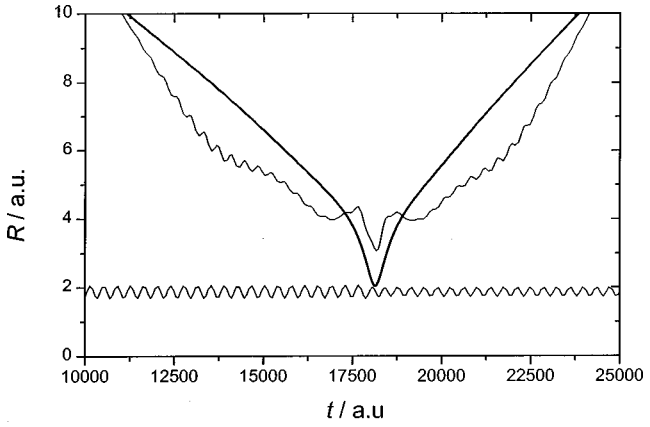

FIG. 6. Example of CT with short-lived HO$_2$ complex and backdissociation HO+O→HO$_2$→HO+O (lower oscillating line=H–O distance, fat line =O–O distance, other line=second H–O distance, 1 a.u.=2.419×10^{-17} s).

The present conclusions about the amount of backdissociation do not agree with the CT results from Ref. 27. This may either originate from differences between the DMBE IV and the present potential, or from different ways to cope with

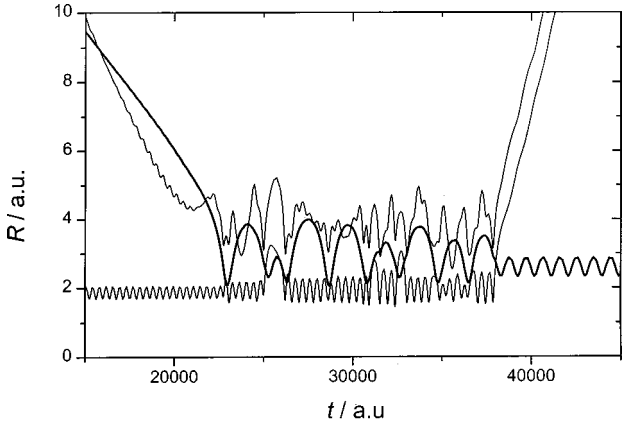

FIG. 7. As Fig. 6, with long-lived HO$_2$ complex and reaction HO+O→HO$_2$→H+O$_2$ (fat line=O–O distance, the two other lines=O–H distances).

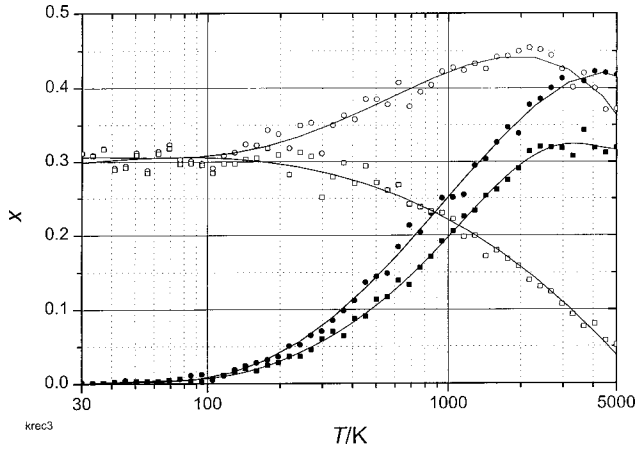

FIG. 8. Fraction x of CTs starting from HO+O which lead to nonstatistical backdissociation (O=CTs starting at quantized vibrational levels of HO, including backdissociation with less than the ZPE, □=part of O leading to backdissociation with less than the ZPE, ■=difference between ○ and □, i.e., allowed backdissociations, ●=CTs with backdissociations starting at zero classical vibrational energy of OH, see text).

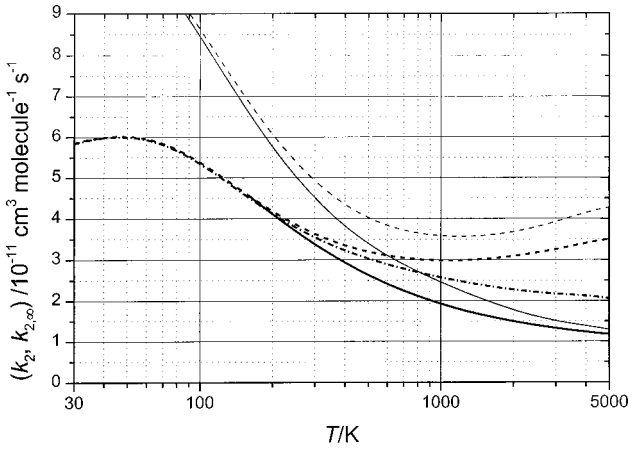

FIG. 10. Classical rate constants $k_{2,\infty}$ and k_2 (lower set of three curves on present potential, upper set of two curves on the DMBE IV potential, dashed curves=$k_{2,\infty}$, full lines=k_2, dashed–dotted curve=k_2 from statistical SACM/CT results of Ref. 8).

the ZPE dilemma. In order to answer this question, we have done CT calculations on the DMBE IV surface following our ZPE correction procedure. Figure 9 compares the sum of statistical and nonstatistical fractions of backdissociation such as calculated with the present and the DMBE IV potential; the statistical fraction from the present work is also shown for illustration. The similarity between the present and the DMBE IV results indicates that the differences between the present work and Ref. 27 must be in the ZPE problem. Indeed the QCT results from Ref. 27, not accounting for ZPE restrictions in order not to create a larger fraction of nonchaotic trajectories, lead to fractions of backdissociating collisions which nearly agree with our results in Fig. 8 including forbidden encounters. On the other hand, the QCT-IEQMT method from Ref. 34, rejecting all $H+O_2$ trajectories leading to HO+O with a total internal energy below the ZPE of HO, seems to be consistent with the present results from Fig. 8, although the earlier work because of the small number of calculated trajectories, showed much larger scatter of the results. While our procedure slightly differs from the QCT-IEQMT method from Ref. 34, it agrees with the ZP3 method from Refs. 35,36 which was applied to the DMBE III potential. Again the larger scatter of this earlier work prevents conclusions about quantitative agreement.

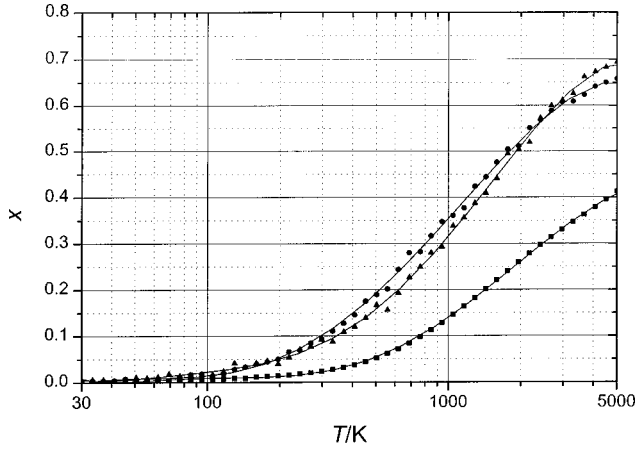

FIG. 9. As Fig. 8, allowed backdissociations (●=as ● in Fig. 8 on the present potential, ▲=the same as ● but on the DMBE IV potential, ■=statistical backdissociations from Ref. 8).

Summarizing our discussion of nonstatistical and statistical backdissociations, we conclude that ZPE restrictions are only mildly influenced by the differences between the DMBE IV and the present potential energy surface. Differences between the calculated k_2 are instead mainly due to different capture rate constants $k_{2,\infty}$. Judging on the basis of the excellent agreement between our results on the experiments such as illustrated in Sec. IV, we tend to believe that the conclusions from Ref. 27 on nearly temperature independent backdissociation ratios from 250 to 5000 K, based on a neglection of the ZPE problem, are in error.

A final remark concerns the behavior of the CTs during the encounters such as illustrated by the examples of Figs. 6 and 7. One may be irritated to see encounters in which the H–O vibration temporarily contains less energy than the ZPE. Anharmonic coupling and lifetime broadenings, however, may well keep such trajectories in the allowed range. It remains an open question whether quantum effects change the character of trajectories from more regular to more chaotic, or whether quantum effects lead trajectories, which in our work end up in the forbidden range, back into the allowed range. Only a comparison with wave packet calculations will provide a final solution of this dilemma. For the moment, one may only hope that the chosen ZPE policy is realistic. The good agreement between calculated k_2 and the experiments demonstrated below seems to support our procedure.

C. CT calculations of k_2

Combining Fig. 9 with Fig. 5 leads to the final results for the classical rate constants k_2 such as shown in Fig. 10. One observes about equal contributions from statistical and nonstatistical backdissociations, lowering k_2 below the capture value $k_{2,\infty}$. While backdissociation is nearly negligible for

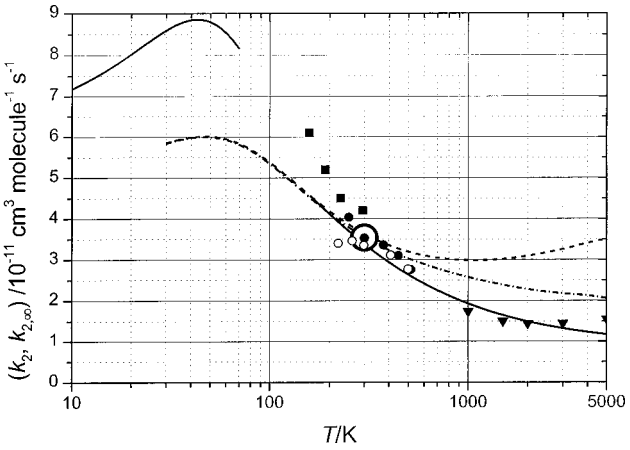

FIG. 11. Comparison of measured and calculated values of k_2 [lower set of three curves=classical calculations from this work and Ref. 8, see Fig. 10, full line up to 70 K=quantum SACM from Ref. 8 with the lowest four channels, ▼=measured k_1 from Eq. (1.6) (Ref. 11) converted to k_2 with K_{eq} from Eq. (1.5), ■=measured k_2 from Ref. 16, ○=measured k_2 from Ref. 15, large circle at 300 K=average k_2 from Refs. 15, 16, 37–39].

300–500 K, it becomes substantial above 1000 K, lowering k_2 below $k_{2,\infty}$ by about a factor of 3 near 5000 K. Our final result for k_2 can be expressed analytically in the form,

$$k_2/10^{-11}\ \text{cm}^3\,\text{molecule}^{-1}\,\text{s}^{-1} = 0.026(T/1000\ \text{K})^{1.47} + 1.92(1000\ \text{K}/T)^{0.46} \quad (3.1)$$

between about 300 and 5000 K. We do not extend this representation to lower temperatures, because quantum effects here change the results.

While the backdissociation ratios from the present and the DMBE IV potentials nearly agree, see Fig. 9, the final rate constants k_2 differ to a larger extent. Figure 10 compares the present with the DMBE IV results. The DMBE IV capture rate constants $k_{2,\infty}$ are substantially larger than the present result, the difference being a factor of 1.52 at 150 K, 1.44 at 300 K, 1.18 at 1000 K, and 1.23 at 5000 K. As mentioned in Sec. II, this difference arises less from differences in the MEP potential, but more from a smaller anisotropy of the DMBE IV potential. It appears worth mentioning that an overestimated $k_{2,\infty}$, combined with an underestimated fraction of reactive CTs, by compensation still can lead to reasonable agreement with experimental data. However, heading for results on the 10%–20% accuracy level over wide ranges of conditions, artifacts of this type have to be eliminated.

IV. DISCUSSION

A. Comparison with experimental results

Figure 11 compares our theoretical results with the available experimental data. The figure includes the capture rate constant $k_{2,\infty}$ from the classical SACM/CT treatment of Ref. 8, the determination of k_2 with statistical backdissociation from the classical SACM/CT treatment of Ref. 8, and the classical results for k_2 from the present work including allowed nonstatistical backdissociations (following the described ZPE policy). In addition, for temperatures below 70 K, capture rate constants $k_{2,\infty}$ from quantum SACM including the lowest four channels[8] are also shown. The quantum SACM results well extrapolate to the low temperature experimental data from Refs. 15 and 16. However, more work including higher channels and accounting for electronically nonadiabatic effects with open shell O($^3P_2$) and OH($^2\Pi_{3/2}$) is required, see part III.[26] The average of the most recent and most direct measurements of k_2 (Refs. 15, 16, 37–39) at 300 K corresponds to $k_2 = 3.54(\pm 0.4)\times 10^{-11}$ cm^3 molecule^{-1} s^{-1}. This value agrees very well with the present result of $k_2 = 3.35\times 10^{-11}$ cm^3 molecule^{-1} s^{-1} from Eq. (3.1). One should, however, keep in mind that some quantum effects may still be present near 300 K.

The optimum experimental values for k_1 apparently are those from Ref. 11 given by Eq. (1.6). Earlier higher values from Ref. 40 seem not to have been confirmed, remeasurements approaching Eq. (1.6).[41] The reasons for some lower results near 2500 K (Ref. 42) are not understood. The conversion of k_1 into k_2 depends on the quality of the equilibrium constant K_{eq}. Using Eqs. (1.5) and (1.6), we obtained the points shown in Fig. 11 such as calculated from

$$k_2/10^{-11}\ \text{cm}^3\,\text{molecule}^{-1}\,\text{s}^{-1} = 0.953(T/1000\ \text{K})^{0.213}\exp(+670\ \text{K}/T). \quad (4.1)$$

This gives values of $(1.86, 1.54, 1.53)\times 10^{-11}$cm^3 molecule^{-1} s^{-1} in comparison to the theoretical values of $(1.95, 1.47, 1.19)\times 10^{-11}$ cm^{-3} molecule^{-1} s^{-1} from Eq. (3.1) for $T=(1000, 2000, 5000)$ K, respectively. The agreement between measurements and calculations between 300 and 5000 K thus appears quite satisfactory.

B. Comparison with quantum scattering calculations

A comparison with measurements of cross sections for reaction (1.1),[17,43–46] and the corresponding quantum scattering calculations from Refs. 17, 29, 30 at present can only be done to a limited extent. The cross-section measurements still show considerable scatter and are not sufficiently precise near threshold to allow for a meaningful conversion into thermal rate constants k_1. On the other hand, one may hope for solutions of the ZPE problem from the quantum scattering calculations. A preliminary comparison can be made between the "total reactions probabilities $P^J(E)$" calculated in Ref. 30 and the corresponding expressions in our treatment. For example, the statistical SACM/CT treatment from Ref. 8 has provided the same quantity [$1-P^J(E)$ was plotted in Fig. 11 from Ref. 8]. Although similar orders of magnitude were derived on average, a much stronger J-dependence arose from the quantum scattering results. The difference may be due to nonstatistical or to quantum effects, with minor effects also coming from the different potentials used. However, the scattering calculations were done with vibrationless and nearly rotationless O_2. Our CT calculations suggested that this limitation can have had a major effect. For this reason, more extended quantum scattering calculations on our new potential are desirable.

One should finally mention that quantum lifetime calculations for highly excited HO_2 have also been made.[47] These calculations lead to highly fluctuating rates. However, on av-

erage, statistical behavior was found with good agreement between quantum and classical results. In spite of the good agreement between measured and calculated values of k_2, such as illustrated in Fig. 11, one therefore may not completely rule out the possibility that reaction (1.2) nevertheless approaches statistical behavior and that other so far neglected effects have to be taken into account.

ACKNOWLEDGMENT

Financial support of the Deutsche Forschungsgemeinschaft (SFB 357 ''Molekulare Mechanismen unimolekularer Prozesse'') is gratefully acknowledged.

[1] J. A. Miller, *26th Symposium (International) on Combustion* (The Combustion Institute, Pittsburgh, 1996), p. 461.
[2] S. Viti, E. Roueff, T. W. Hartquist, G. Pineau des Forêts, and D. A. Williams, Astron. Astrophys. **370**, 557 (2001).
[3] D. L. Baulch, C. J. Cobos, R. A. Cox, C. Esser, P. Frank, Th. Just, J. A. Kerr, M. J. Pilling, J. Troe, R. W. Walker, and J. Warnatz, J. Phys. Chem. Ref. Data **21**, 411 (1992).
[4] R. Atkinson, D. L. Baulch, R. A. Cox, R. F. Hampson, J. A. Kerr, M. J. Rossi, and J. Troe, J. Phys. Chem. Ref. Data **26**, 1329 (1997).
[5] N. Cohen and K. R. Westberg, J. Phys. Chem. Ref. Data **12**, 531 (1983).
[6] D. L. Baulch, C. J. Cobos, R. A. Cox, P. Frank, G. Hayman, Th. Just, J. A. Kerr, T. Murrells, M. J. Pilling, J. Troe, R. W. Walker, and J. Warnatz, J. Phys. Chem. Ref. Data **23**, 847 (1994).
[7] J. Troe, *22nd Symposium (International) on Combustion* (The Combustion Institute, Pittsburgh, 1988), p. 843.
[8] L. B. Harding, A. I. Maergoiz, J. Troe, and V. G. Ushakov, J. Chem. Phys. **113**, 11019 (2000) (part I of this series).
[9] B. Ruscic, D. Feller, D. A. Dixon, K. A. Peterson, L. B. Harding, R. L. Asher, and A. F. Wagner, J. Phys. Chem. A **105**, 1 (2001).
[10] Expression from Ref. 8, modified with the revised enthalpy of formation of HO from Ref. 9.
[11] H. Du and J. P. Hessler, J. Chem. Phys. **96**, 1077 (1992).
[12] A. N. Pirraglia, J. V. Michael, J. W. Sutherland, and R. B. Klemm, J. Phys. Chem. **93**, 282 (1989).
[13] D. A. Masten, R. K. Hanson, and C. T. Bowman, J. Phys. Chem. **94**, 7119 (1990).
[14] K. S. Shin and J. V. Michael, J. Chem. Phys. **95**, 262 (1991).
[15] M. J. Howard and I. W. M. Smith, J. Chem. Soc., Faraday Trans. 2 **77**, 997 (1981).
[16] I. W. M. Smith and D. W. A. Stewart, J. Chem. Soc., Faraday Trans. **90**, 3221 (1994).
[17] M. A. Bajeh, E. M. Goldfield, A. Hanf, Ch. Kappel, A. J. H. M. Meijer, H.-R. Volpp, and J. Wolfrum, J. Phys. Chem. A **105**, 3359 (2001).
[18] M. R. Pastrana, L. A. M. Quintales, J. Brandão, and A. J. C. Varandas, J. Phys. Chem. **94**, 8073 (1990).
[19] B. Kendrick and R. T. Pack, J. Chem. Phys. **102**, 1994 (1995).
[20] C. F. Melius and R. J. Blint, Chem. Phys. Lett. **64**, 183 (1979).
[21] S. P. Walch, C. M. Rohlfing, C. F. Melius, and C. W. Bauschlicher, J. Chem. Phys. **88**, 6273 (1988); **90**, 7613 (1989).
[22] S. P. Walch and C. M. Rohlfing, J. Chem. Phys. **91**, 2373 (1989).
[23] S. P. Walch and R. J. Duchovic, J. Chem. Phys. **94**, 7068 (1991).
[24] L. B. Harding, J. Troe, and V. G. Ushakov, Phys. Chem. Chem. Phys. **3**, 2630 (2001).
[25] J. Troe, J. Chem. Phys. **105**, 6249 (1996).
[26] A. I. Maergoiz and J. Troe, J. Chem. Phys. (in preparation) (part III of this series).
[27] J. A. Miller and B. C. Garrett, Int. J. Chem. Kinet. **29**, 275 (1997); J. A. Miller and S. J. Klippenstein, *ibid.* **31**, 753 (1999).
[28] R. T. Pack, E. A. Butcher, and G. A. Parker, J. Chem. Phys. **102**, 5998 (1995).
[29] A. J. H. M. Meijer and E. M. Goldfield, J. Chem. Phys. **108**, 5404 (1998); **110**, 870 (1999).
[30] E. M. Goldfield and A. J. H. M. Meijer, J. Chem. Phys. **113**, 11055 (2000).
[31] L. B. Harding, J. Troe, and V. G. Ushakov, Phys. Chem. Chem. Phys. **2**, 631 (2000).
[32] J. M. C. Marques and A. J. C. Varandas, Phys. Chem. Chem. Phys. **3**, 505 (2001).
[33] A. I. Maergoiz, E. E. Nikitin, J. Troe, and V. G. Ushakov, J. Chem. Phys. **108**, 5265,9987 (1998).
[34] A. J. C. Varandas, J. Brandão, and M. R. Pastrana, J. Chem. Phys. **96**, 5137 (1992).
[35] J. Davidsson and G. Nyman, J. Chem. Phys. **92**, 2407 (1990).
[36] G. Nyman and J. Davidsson, J. Chem. Phys. **92**, 2415 (1990).
[37] R. S. Lewis and R. T. Watson, J. Phys. Chem. **84**, 3495 (1980), ''best fit data'' chosen.
[38] F. Temps, Ph.D. dissertation, University of Göttingen, Germany, 1983.
[39] W. H. Brune, J. J. Schwab, and J. A. Anderson, J. Phys. Chem. **87**, 4503 (1983).
[40] P. Frank and Th. Just, Ber. Bunsenges. Phys. Chem. **89**, 181 (1985).
[41] Th. Just (private communication, 2001).
[42] T. Yuan, C. Wang, C.-L. Yu, M. Frenklach, and M. J. Rabinovitz, J. Phys. Chem. **95**, 1258 (1991).
[43] K. Kessler and K. Kleinermanns, J. Chem. Phys. **97**, 374 (1992).
[44] S. Seeger, V. Sick, H.-R. Volpp, and J. Wolfrum, Isr. J. Chem. **34**, 5 (1994).
[45] W. J. van der Zande, R. Zhang, R. N. Zare, K. G. McKendrick, and J. J. Valentini, J. Phys. Chem. **95**, 5 (1991); **95**, 8205 (1991).
[46] H.-G. Rubahn, W. J. van der Zande, R. Zhang, M. J. Bronikowski, and R. N. Zare, Chem. Phys. Lett. **186**, 154 (1991).
[47] M. Stumpf, A. J. Dobbyn, D. H. Mordaunt, H.-M. Keller, H. Fluethmann, R. Schinke, H.-J. Werner, and K. Yamashita, Faraday Discuss. **102**, 193 (1995).